AIP | Review of Scientific Instruments

Development of real-time rotating waveplate Stokes polarimeter using multi-order retardation for ITER poloidal polarimeter

R. Imazawa, Y. Kawano, T. Ono, and K. Itami

Citation: Review of Scientific Instruments **87**, 013503 (2016); doi: 10.1063/1.4939444
View online: http://dx.doi.org/10.1063/1.4939444
View Table of Contents: http://scitation.aip.org/content/aip/journal/rsi/87/1?ver=pdfcov
Published by the AIP Publishing

Development of real-time rotating waveplate Stokes polarimeter using multi-order retardation for ITER poloidal polarimeter

R. Imazawa,[a] Y. Kawano, T. Ono, and K. Itami
Japan Atomic Energy Agency, 801-1 Mukoyama, Naka, Ibaraki, Japan

(Received 1 July 2015; accepted 19 December 2015; published online 8 January 2016)

The rotating waveplate Stokes polarimeter was developed for ITER (International Thermonuclear Experimental Reactor) poloidal polarimeter. The generalized model of the rotating waveplate Stokes polarimeter and the algorithm suitable for real-time field-programmable gate array (FPGA) processing were proposed. Since the generalized model takes into account each component associated with the rotation of the waveplate, the Stokes parameters can be accurately measured even in unideal condition such as non-uniformity of the waveplate retardation. Experiments using a He-Ne laser showed that the maximum error and the precision of the Stokes parameter were 3.5% and 1.2%, respectively. The rotation speed of waveplate was 20 000 rpm and time resolution of measuring the Stokes parameter was 3.3 ms. Software emulation showed that the real-time measurement of the Stokes parameter with time resolution of less than 10 ms is possible by using several FPGA boards. Evaluation of measurement capability using a far-infrared laser which ITER poloidal polarimeter will use concluded that measurement error will be reduced by a factor of nine. © *2016 AIP Publishing LLC.* [http://dx.doi.org/10.1063/1.4939444]

I. INTRODUCTION

A poloidal polarimeter system will be installed in International Thermonuclear Experimental Reactor (ITER) to identify a safety factor profile, $q(r)$, in a plasma core region.[1] The ITER poloidal polarimeter will use a far-infrared laser (wavelength is 119 μm) as a probing laser to measure both the Faraday effect and the Cotton-Mouton effect.[2] The Faraday effect rotates a polarization ellipse, and the Cotton-Mouton effect changes an ellipticity of the polarization ellipse. Thus, a method for measuring both an orientation angle and an ellipticity angle of a polarization state needs to be applied to the ITER poloidal polarimeter. The authors have investigated several polarization measurement techniques. Considering not only a measurement capability but also reliability, availability, and maintainability, the authors concluded that a rotating waveplate Stokes polarimeter is most appropriate for the ITER poloidal polarimeter.[3]

Baseline technical specifications of accuracy of measuring the polarization state are 1° for the orientation angle and 6° for the ellipticity angle. According to Ref. 2, the specifications of the accuracy enable the poloidal polarimeter to identify q-profile of ITER inductive scenario plasma with 10% accuracy. The accuracy includes all error sources such as calibration error and polarization change caused by in-vessel retro-reflector. In order to allow larger error due to the calibration error and the polarization change due to the retro-reflector, the authors decided that target standard errors of only the rotating waveplate Stokes polarimeter are 0.05° for the orientation angle and 0.3° for the ellipticity angle. This target standard error would enable the ITER poloidal polarimeter to contribute to successful experiments of steady-state operation scenario with negative magnetic shear configuration. Technical specifications of a time resolution are 10 ms for off-line data analysis[4] and 100 ms for real-time measurement, but a target specification of this study is 10 ms for the real-time measurement. (This is because a data analysis procedure of the ITER poloidal polarimeter will avoid re-analyzing raw data to prepare off-line data after a long plasma discharge of 1000 s. The raw data of 1000-s discharge could be more than 400 GB per viewing chord.)

The rotating waveplate Stokes polarimeter consists of a rotating quarter waveplate and a linear polarizer. Detector signal is modulated by the rotation of the quarter waveplate and Fourier analysis of the detector signal provides information identifying the polarization state. It is a well-known technique in a field of polarimetry, but there is no rotating waveplate Stokes polarimeter measuring at the time resolution of 10 ms in real time. Theory of the rotating waveplate Stokes polarimeter is simple, but practice with high accuracy is not simple under unideal conditions such as concentric distribution of birefringence and non-flatness and wedged shape of the waveplate.

This study will propose a generalized model of analyzing the rotating waveplate Stokes polarimeter and an algorithm suitable for real-time data analysis. The generalized model takes into account of the unideal conditions mentioned above. Experiments using a He-Ne laser (in other words, experiments using low waveplate quality) will demonstrate a performance of the proposed methods and will give positive perspectives of measurement capability using a far-infrared laser.

II. MEASUREMENT METHOD

A. Theory including unideal waveplate and right-angle mirror

The conventional rotating waveplate polarimeter needs a high-rotation-speed air spindle with a hollow axis. Although the high-rotation-speed air spindle with a hollow axis is

[a]Electronic mail: imazawa.ryota@jaea.go.jp

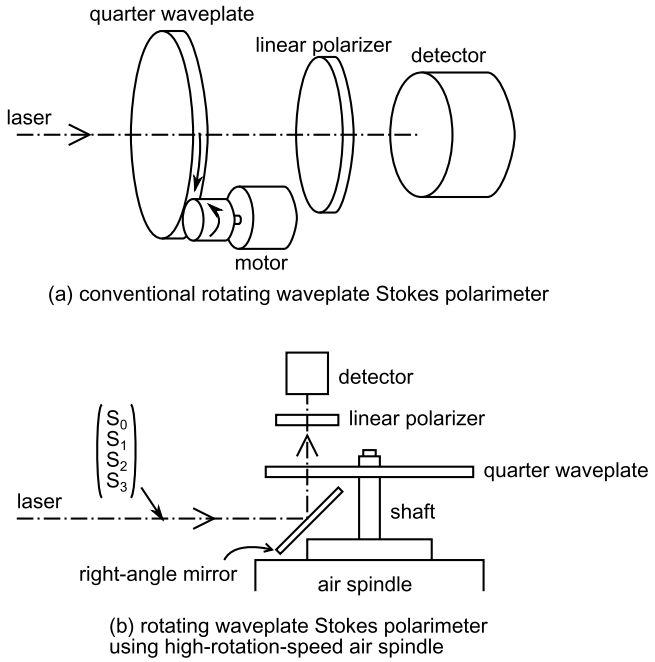

FIG. 1. Schematics of rotating waveplate polarimeter. In comparison with the conventional method, the polarimeter using high-rotation-speed air spindle includes a right-angle mirror in front of a quarter waveplate.

commercially available,[3,5] available hollow diameter is limited (e.g., 20000 rpm rotation with the hollow diameter of 20 mm or more is not available). The authors develop a rotating waveplate polarimeter using high-rotation-speed air spindle without the hollow axis. Fig. 1 illustrates the conventional rotating waveplate Stokes polarimeter and the developed rotating waveplate polarimeter using high-rotation-speed air spindle. In comparison with the conventional method, this schematics include a right-angle mirror in front of a quarter waveplate. Since the right-angle mirror makes a method for analyzing a detector signal different from the conventional one, this section will explain the analysis method considering the right-angle mirror.

A detector signal of the conventional rotating waveplate method is typically given by

$$F(t) = \frac{S_0}{2} + \frac{S_1}{4} + \frac{S_1}{4}\cos 4\omega t + \frac{S_2}{4}\sin 4\omega t - \frac{S_3}{2}\cos 2\omega t, \quad (1)$$

where (S_0, S_1, S_2, S_3) is Stokes parameters to be measured and ω is an angular velocity of the waveplate. When a light is fully polarized, the relation between Stokes parameters and the angular parameters (i.e., the orientation and the ellipticity angle) is given by

$$\begin{pmatrix} S_0 \\ S_1 \\ S_2 \\ S_3 \end{pmatrix} = S_0 \begin{pmatrix} 1 \\ \cos 2\epsilon \cos 2\psi \\ \cos 2\epsilon \sin 2\psi \\ \sin 2\epsilon \end{pmatrix}, \quad (2)$$

where ψ and ϵ denote the orientation and the ellipticity angle, respectively. Further relation between change of the Stokes parameters in plasmas and change of the angular parameters in plasma can be found in Ref. 6. When thermal stress and/or centrifugal force causes concentric distribution of birefringence, the retardation that the light receives during the rotation of the quarter waveplate is expressed by $\pi/2 + \delta\cos(2\omega t)$. Thus, the equation of the detector signal is more complicated as follows:

$$\begin{aligned} F(t) = \frac{S_0}{2} &+ \left[1 - 2\sum_n J_{2n-1}(\delta)\sin\{(2n-1)2\omega t\}\right]\frac{S_1}{4} \\ &+ \left[1 + 2\sum_n J_{2n-1}(\delta)\sin\{(2n-1)2\omega t\}\right]\frac{S_1}{4}\cos 4(\omega t) \\ &+ \left[1 + 2\sum_n J_{2n-1}(\delta)\sin\{(2n-1)2\omega t\}\right]\frac{S_2}{4}\sin 4(\omega t) \\ &- \left[J_0(\delta) + 2\sum_n J_{2n}(\delta)\cos\{2n2\omega t\}\right]\frac{S_3}{2}\cos 2(\omega t), \end{aligned} \quad (3)$$

where J_n is the first kind of Bessel function. In addition, taking into account a polarization-dependency of reflectance of the right-angle mirror (see Fig. 1) and non-flatness of waveplate and distribution of birefringence, the detector signal becomes more complicated. A generalized description below is useful for avoiding the complexity,

$$F(t) = S_0 \sum_i \{a_i \cos(i\omega t) + b_i \sin(i\omega t)\}, \quad (4)$$

$$a_i = X_{i0} + X_{i1}s_1 + X_{i2}s_2 + X_{i3}s_3, \quad (5)$$

$$b_i = Y_{i0} + Y_{i1}s_1 + Y_{i2}s_2 + Y_{i3}s_3, \quad (6)$$

where $\vec{s} = (s_1, s_2, s_3)$ is the reduced Stokes parameter (i.e., $\|\vec{s}\| = 1$). In other words, this expression expands Mueller matrix in terms of Fourier series. Let $M = \{M_{ij}\}$ $(i, j = 0, \ldots, 3)$ denote Mueller matrix taking into account the right-angle mirror, the unideal waveplate, and the polarizer. The first row of the Mueller matrix can be expressed by

$$M_{0j} = \sum_i \{X_{ij}\cos(i\omega t) + Y_{ij}\sin(i\omega t)\}. \quad (7)$$

It should be noted that the element of X_{i0} and Y_{i0} comes from the right-angle mirror. Thus, if the laser can pass through waveplate without the right-angle mirror, X_{i0} and Y_{i0} are zero.

The authors do not give an explicit description of $X\,(=\{X_{ij}\})$ and $Y\,(=\{Y_{ij}\})$ using physical parameters mentioned above such as non-flatness of waveplate. The values of X and Y are determined by a calibration. Besides, in the calibration phase, an experimenter determines which mode (i.e., i in Eq. (4)) has high sensitivity to Stokes parameters. For example, if the waveplate ideally has a retardation of $\pi/2$, only the 2nd and 4th modes ($i = 2, 4$ in Eq. (4)) have sensitivity to Stokes parameters. If the waveplate is wedge-shaped, the fundamental mode ($i = 1$ in Eq. (4)) has sensitivity as well.

After the calibration and the sensitivity assessment are finished, an experimenter can measure the Stokes parameters, $\vec{s}$, in accordance with steps below: (step 1) measuring $F(t)$, (step 2) identifying $\vec{a}$ and $\vec{b}$ by using Fourier analysis, and (step 3) solving simultaneous linear equations,

$$\begin{pmatrix} \vec{a} \\ \vec{b} \end{pmatrix} = \begin{bmatrix} X \\ Y \end{bmatrix} \vec{s}. \quad (8)$$

B. Algorithm of real-time data analysis suitable for field-programmable gate array (FPGA)

It is necessary to identify Fourier coefficients, $\vec{a}$ and $\vec{b}$, accurately for the sake of accurate measurement of Stokes parameters. Intensity of low modes such as $\sin 2\omega t$ or $\sin 4\omega t$ is larger than that of high modes. Although FFT (fast Fourier transform) is well-known algorithm to identify Fourier coefficients, FFT does not suit for identifying low modes from measurement data during one rotation cycle (i.e., $0 \le t < 2\pi/\omega$). Only when the total number of samples can be expressed by power of two, FFT of measurement data during one rotation provides accurate result of low modes. As described later (Section III), the total number of samples during one rotation cycle is 825 000 under experimental conditions of this study and would lead to 10% error of amplitude of fundamental mode even without measurement error. Thus, the authors propose numerical calculation of integrals below,

$$\begin{cases} a_i = \dfrac{\pi}{\omega}\displaystyle\int_0^{2\pi/\omega} F(t)\cos(i\omega t)\mathrm{d}t, \\ b_i = \dfrac{\pi}{\omega}\displaystyle\int_0^{2\pi/\omega} F(t)\sin(i\omega t)\mathrm{d}t. \end{cases} \tag{9}$$

As already mentioned in Section II A, since the sensitivity assessment is carried out during calibration, the total number of i to be calculated is limited.

The final goal of this study is the real-time measurement of Stokes parameters as mentioned in Section I. It is preferable to calculate Eq. (9) in real time by using FPGA. Since air spindle has an encoder for accurate control of rotation speed, A-phase and Z-phase signals of the encoder can be used to obtain a phase angle of the rotating waveplate and the integral interval, respectively. The phase angle, ωt, is approximately given by $\omega t \approx 2\pi k/2^N$, where k is a total number of A-phase pulses that are detected after Z-phase pulse is detected, and N is a bit number of the encoder. The issue of real-time calculation of Eq. (9) in FPGA is that the computational cost of the sine and cosine functions is high. In order to avoid calculating the sine and cosine functions, the basis functions of the series expansion of Mueller matrix are changed from $\sin(i\omega t)/\cos(i\omega t)$ to $\mathrm{sgn}\{\sin(i\omega t)\}/\mathrm{sgn}\{\cos(i\omega t)\}$, where $\mathrm{sgn}(x)$ denotes a sign of x. The detector signal is given by

$$F(t) = S_0 \sum_i \left[a_i \mathrm{sgn}\{\cos(i\omega t)\} + b_i \mathrm{sgn}\{\sin(i\omega t)\}\right], \tag{10}$$

where the definition of a_i and b_i is identical with Eqs. (5) and (6). Mathematical comments on the justification of the new basis functions can be found in the Appendix of this paper. The value of $\mathrm{sgn}\{\sin(i\omega t)\}/\mathrm{sgn}\{\cos(i\omega t)\}$ can be evaluated by conditional branching, of which the computational cost is cheaper than that of the sine and cosine functions. For example, $\mathrm{sgn}\{\cos(2\omega t)\}$ can be evaluated as follows:

$$\mathrm{sgn}\{\cos(2\omega t)\} = \begin{cases} 1 & 0 \le k < 2^{N-2} \\ -1 & 2^{N-2} \le k < 2^{N-1} \\ 1 & 2^{N-1} \le k < 3\cdot 2^{N-1} \\ -1 & 3\cdot 2^{N-2} \le k < 2^N \end{cases}. \tag{11}$$

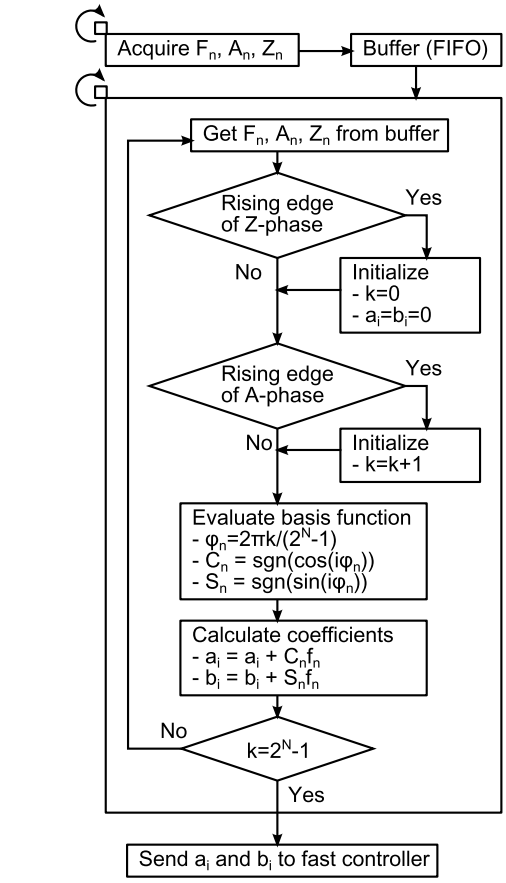

FIG. 2. Flowchart of algorithm of calculating series expansion coefficients, a_i and b_i, in FPGA. F_n, A_n, and Z_n denote the detector signal, A-phase signal of the encoder, and Z-phase signal of the encoder, respectively, Eqs. (5) and (6). The value of $\mathrm{sgn}\{\sin(i\phi_n)\}/\mathrm{sgn}\{\cos(i\phi_n)\}$ can be evaluated by conditional branching.

Fig. 2 summarizes the proposed algorithm suitable for real-time data analysis in FPGA. As mentioned in Section II A, an experimenter needs to solve the simultaneous equations, $\vec{a} = X\vec{s}$ and $\vec{b} = Y\vec{s}$. The calculation of solving the simultaneous equations is carried out by a fast controller (such as personal computer (PC)), not by FPGA. Fig. 3 shows the overview of the real-time rotating waveplate Stokes polarimeter using the high-rotation-speed air spindle.

III. EXPERIMENTAL SETUP

We made experiments to demonstrate that the measurement method proposed in Section II has potential ability

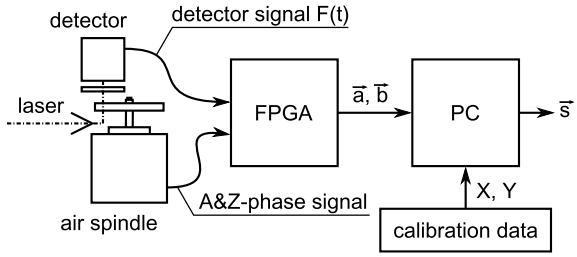

FIG. 3. Overview of the real-time rotating waveplate Stokes polarimeter using the high-rotation-speed air spindle.

of measuring Stokes parameters with high accuracy and high time resolution. ITER poloidal polarimeter uses a far-infrared laser (wavelength is 119 μm). However, since the authors have no light source in far-infrared region, the authors made experiments by using a He-Ne laser (wavelength is 632.8 nm). Major error sources of the rotating waveplate method are laser power fluctuation and oscillation of optical components which are not synchronized with the rotation of the waveplate. The laser power fluctuation of the He-Ne laser was 1% during 1000 s. ITER poloidal polarimeter plans to use a far-infrared laser developed by Chubu University.[7,8] The Chubu University achieved stability of 1% with about an output power of about 1 W for a long-term operation of 24 h.[9] Thus, it is proper to use the He-Ne laser for the experiments assessing the performance of the rotating waveplate polarimeter. Regarding unsynchronized oscillation of components, measurement error using the He-Ne laser is larger than that using the far-infrared laser because amplitude of unsynchronized oscillation normalized by wavelength of the He-Ne laser is larger than that of the far-infrared laser.

A. Design of quartz waveplate

A quarter waveplate for both the He-Ne laser and the far-infrared laser is made of quartz. Since the quarter waveplate will be rotated in the manner shown in Fig. 1, a shape of the waveplate is a disk and has a hole at the center for fixation. For the sake of easier fabrication of the hole, a thickness of quartz needs to be around 2.5 mm. That is to say, it is inevitable to use multi-order quarter waveplate for the rotating waveplate with configuration shown in Fig. 1. The specifications of the quarter waveplate used in this experiment are as follows: diameter of 50 mm, hole diameter (D) of 6 mm, parallelism (θ) of 5 s, and flatness of 0.158 μm. Thus, key parameters normalized by wavelength, λ(= 632.8 nm), are as follows: retardation of $\lambda/4$ (36th order), flatness of $\lambda/4$, and wedge height ($h = D\tan\theta$) of 1.9λ.

When the quarter waveplate rotates, the maximum stress is applied to the circumference of the central hole. Assuming that the allowable stress of quartz is the same as that of fused silica, the allowable stress is approximately 40 MPa. Setting a safety margin to 10, the quarter waveplate with the size mentioned above needs to rotate at a speed of less than 23 000 rpm.

B. Air spindle

An air spindle of ShinMaywa Industries, Ltd. (SPM27H) was used. The air spindle can rotate at a maximum speed of 20 000 rpm and the rotation speed fluctuation is 0.01%. Resolution of the encoder is 9 bits. The unsynchronized run-out of the air spindle shaft was 6 nm in the axial direction and 7 nm in the radial direction. The unsynchronized run-out of the quarter waveplate rotated by the air spindle is unknown.

Since the air spindle rotation speed is 20 000 rpm, the time resolution of measuring the Stokes parameters is 3.3 ms (333 Hz). It is better than the requirement of ITER poloidal polarimeter (10 ms).

C. Analog-digital converter (ADC) resolution

In ITER, instrumentation and control devices are standardized and candidates of the FPGA boards are limited. ITER poloidal polarimeter plans to use a FPGA instrument with sampling rate of 250 MHz and ADC voltage resolution of 14 bits. However, the authors do not have this FPGA instrument. This study uses an oscilloscope with sampling rate of 250 MHz and voltage resolution of 11 bits in order to verify the high-speed Stokes parameter measurement off-line. Assessment of FPGA performance will be discussed in Section V by using software emulation.

IV. EXPERIMENTAL RESULTS

A. Contribution of centrifugal force to birefringence

Linear polarized light was measured with different rotation speed in order to confirm contribution of the centrifugal force to birefringence of the waveplate. Fig. 4 shows the power spectrum of the detector signal in the condition of different rotation speed. Although centrifugal force of 333 Hz rotation speed is 10 times higher than that of 100 Hz, change of the spectrum intensity is small. Therefore, it is concluded that the contribution of the centrifugal force to the birefringence of the waveplate is negligible.

B. Thermal effect to birefringence

Linear polarized light was measured with different waveplate temperatures in order to confirm thermal effect to birefringence of the waveplate. The thermal effect includes

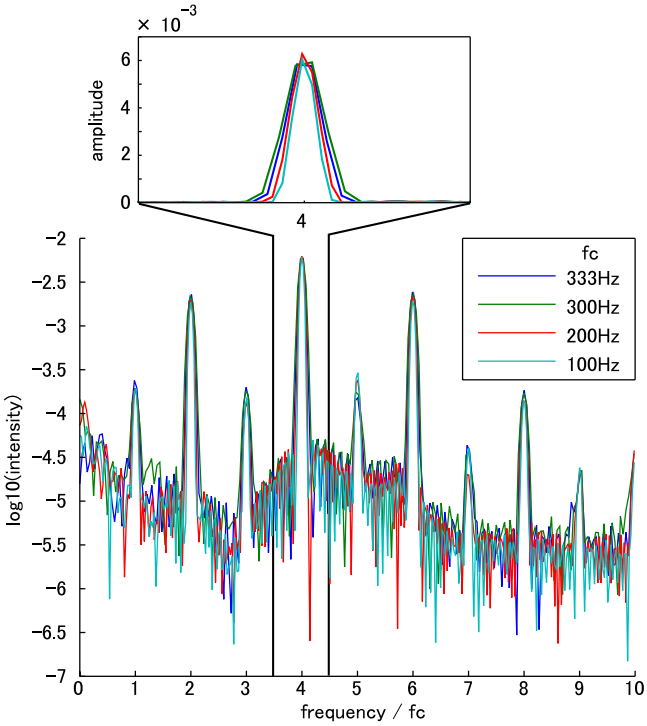

FIG. 4. Power spectrum of the detector signal. Linear polarized light of the He-Ne laser was measured with different rotation speed. f_c denotes rotation speed of the air spindle.

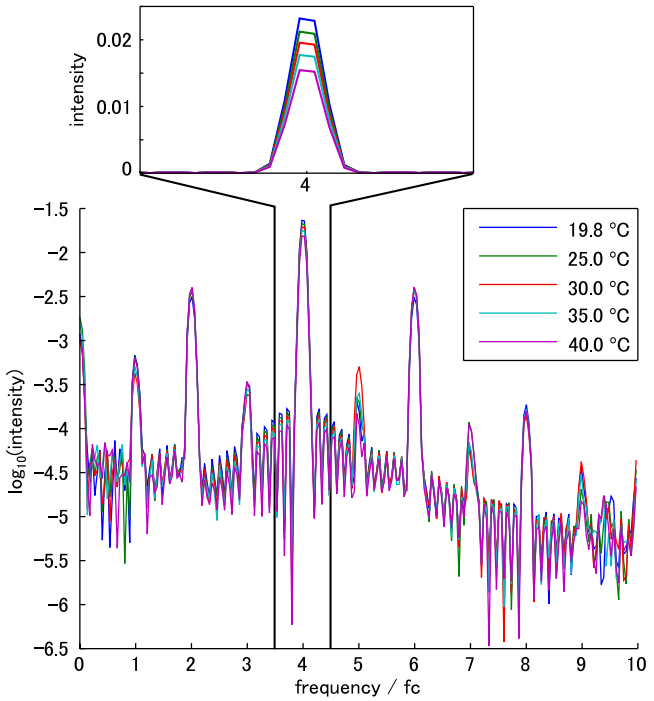

FIG. 5. Power spectrum of the detector signal. Linear polarized light of the He-Ne laser was measured with different waveplate temperatures. f_c denotes rotation speed of the air spindle (it was 20 000 rpm).

thermal stress and temperature-dependency of refractive index. Fig. 5 shows the power spectrum of the detector signal in the condition of different temperatures and the temperature in the figure expresses the temperature of air-spindle housing. The rotation speed was 20 000 rpm. When the air spindle starts, the temperature increases. Fig. 5 shows different time snapshots during the temperature increase. The power spectrum clearly depends on the temperature. In Section IV A, the finite difference between the spectrum intensity of 100 Hz and 333 Hz rotation would come from the change of waveplate temperature, which is associated to the rotation speed (i.e., the electrical power consumption).

Fig. 6 shows the temperature distribution measured by an infrared camera. The temperature of shaft was the highest. It is supposed that the heat was conducted from the shaft to the waveplate and the temperature of the waveplate was not uniform. At the moment, thermal stress is unknown.

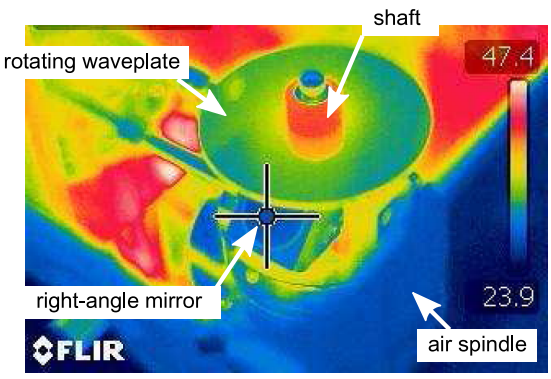

FIG. 6. Temperature distribution measured by an infrared camera.

C. Sensitivity assessment and accuracy assessment

By using a reference of a polarization state, a sensitivity assessment and an accuracy assessment were carried out. The reference of the polarization state was linear or elliptic polarization state made by combination of the polarizer and the quarter waveplate (the polarizer and the quarter waveplate for the reference are different from those for the rotating waveplate polarimeter). The reference of the polarization state was used for both calibration and test data. The calibration data are used for determining the value of X and Y. The test data are used for evaluating accuracy of the rotating waveplate polarimeter. The reference of the polarization state covered the polarization orientation angle between −60° and 60° and the ellipticity angle between −40° and 45°.

As mentioned in Section III C, this experiment used the oscilloscope and data analysis was carried out by a desktop PC, not by FPGA. However, the data analysis method is the same as that proposed in Section II B. The rotation speed of waveplate was 20 000 rpm and the time resolution of measuring the Stokes parameters is 3.3 ms (333 Hz).

First, the authors investigated which combination of three modes from the first to eighth modes was most accurate. The result was that the combination of the 1st, 5th, and 6th modes was most accurate. Next, the authors investigated which additional mode improves the accuracy. The result was that the 8th mode improved the accuracy most. In other words, when four modes are used for data analysis, the best combination is the 1st, 5th, 6th, and 8th modes. Similarly, the author investigated if additional modes improve the accuracy. Finally, the authors concluded that the best combination is the 1st, 5th, 6th, 7th, and 8th modes. It should be noted that the accuracy using this best combination is better than that using all modes from the 1st to 8th modes. The maximum error of Stokes parameter was 3.5% in the case of the best combination.

D. Long-term stability

The horizontal linear polarization state was measured for 1000 s. Fig. 7 shows the results. The time resolution of measuring the Stokes parameter was 3.3 ms. The 1st, 5th, 6th, 7th, and 8th modes were used for data analysis. The results clearly show that there is no drift of measurement data and that the laser power fluctuation of 1% does not effect

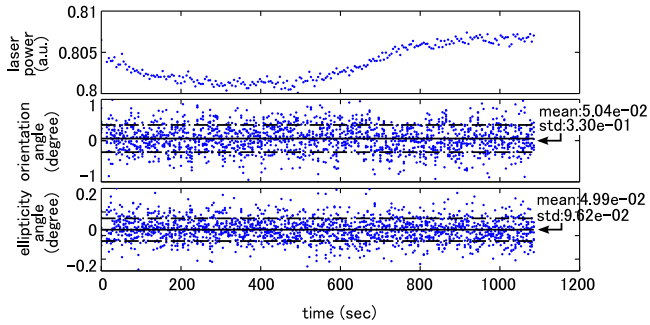

FIG. 7. Result of measuring horizontal linear polarization state for 1000 s. The upper, middle, and lower plots show time evolution of laser power, orientation angle, and ellipticity angle, respectively. "mean" and "std" in plots denote the mean value and the standard deviation of data, respectively.

the polarization measurement. The achieved precision of the orientation angle, ellipticity angle, and the Stokes parameter was 0.33°, 0.096°, and 1.2%, respectively.

V. ASSESSMENT OF FPGA PERFORMANCE

Since higher time resolution leads to more accurate numerical integral of data with noise, this method requires a high-speed sampling ADC. The authors carried out software emulation to clarify compatibility of the high-speed sampling and calculation of the proposed algorithm (Section II B) in FPGA processing. Software of LabVIEW FPGA Module (National Instruments Corporation) was used. Frequency margin of 1.83 MHz and slices margin of 68.5% were confirmed. The result shows that two modes (a_i, b_i, a_j, and b_j) can be simultaneously calculated at a sampling frequency of 250 MHz. Thus, when the 1st, 5th, 6th, 7th, and 8th modes are used for data analysis, three FPGA boards are necessary for 250 MHz sampling. Otherwise, the sampling rate needs to be reduced.

VI. DISCUSSION

The experiments above used the He-Ne laser (632.8 nm). If the far-infrared laser (119 μm) was used, achievement of higher accuracy is expected. The method proposed in Section II takes into account each component associated with the rotation of the waveplate. The amplitude of unsynchronized oscillation of optical components normalized by 119 μm is smaller than that normalized by 632.8 nm. In addition, the waveplate quality of the quarter waveplate is significantly improved, when the wavelength is changed from 632.8 nm to 119 μm. Table I shows the comparison of the quality of 632.8 nm and 119 μm. Since the order of retardation is reduced by a factor of nine, the error associated with unsynchronized run-out of the waveplate will be reduced by a factor of nine.

The best combination of modes used for data analysis of the rotating waveplate method was explained in Section IV C, but depends on instruments. Our result shows that the combination of the 1st, 5th, 6th, 7th, and 8th modes is best. Signal fluctuation unsynchronized with the rotation of the quarter waveplate happened to have the 2nd, 3rd, and 4th harmonic components. When much lower parallelism of waveplate is available, the 1st mode is excluded from the best combination. As shown in Table I, the wedge height normalized by wavelength will be decreased, the best combination will be different from the result of He-Ne laser.

TABLE I. Comparison of quarter waveplate quality. The material of the waveplate is quartz and thickness is supposed to be around 2.5 mm. Definition of the wedge height can be found in Section III A.

	$\lambda = 632.8$ nm	$\lambda = 119$ μm
Order of retardation	36	4
Flatness	$\lambda/4$	$\lambda/753$
Wedge height	1.9λ	$\lambda/100$

Since the total number of modes used for the data analysis is unknown, the necessary number of FPGA board for 250 MHz sampling is also an open question.

If the 1st mode will not be used for the data analysis, the Stokes parameter can be calculated every half rotation of the waveplate. Thus, there is a possibility of improving the time resolution of measuring the Stokes parameter, even if the same instruments are used for measuring the far-infrared light.

Section I explained that the motivation of this study is the development of the ITER poloidal polarimeter and the target standard errors of the ITER poloidal polarimeter are about 0.05° for the orientation angle and 0.3° for the ellipticity angle. It is difficult to conclude that the results of this study meet the target performance because the target performance is not adequate. When the polarization state is nearly circular, the error of the orientation angle would be a few degrees, while the error of the Stokes parameters is less than 1%. Therefore, the target performance should be specified in terms of the Stokes parameters, not the orientation and ellipticity angles. The improvement of the specification is beyond the scope of this paper and needs to consider ITER plasma operation scenarios.

VII. CONCLUSIONS AND FUTURE WORKS

The rotating waveplate Stokes polarimeter was developed for ITER poloidal polarimeter. The generalized model of the rotating waveplate Stokes polarimeter (Eq. (10)) and the algorithm suitable for FPGA processing were proposed. Since the generalized model takes into account each component associated with the rotation of the waveplate, the Stokes parameters can be accurately measured even in unideal condition such as non-uniformity of the waveplate retardation.

The performance was assessed by using the He-Ne laser (λ = 632.8 nm) using the quarter waveplate of 36th order retardation, $\lambda/4$ flatness, and 1.9λ wedge height. The maximum error and the precision of the Stokes parameter were 3.5% and 1.2%, respectively. The rotation speed of waveplate was 20 000 rpm and time resolution of measuring the Stokes parameter was 3.3 ms.

The compatibility of the high-speed sampling and calculation of the proposed algorithm in FPGA processing were evaluated. The result shows that two modes (a_i, b_i, a_j, and b_j) can be simultaneously calculated at a sampling frequency of 250 MHz. In principle, the real-time measurement of the Stokes parameter with time resolution of less than 10 ms is possible by using several FPGA boards.

If the far-infrared laser (119 μm) that ITER poloidal polarimeter will use was available for the performance assessment of the rotating waveplate Stokes polarimeter, higher accuracy could be achievable because the quality of waveplate normalized by wavelength is higher and amplitude of unsynchronized run-out normalized by wavelength is smaller. The performance assessment using the far-infrared laser is necessary for confirming not only the positive effect of the waveplate quality but also the effect related to the beam quality and will be a future work.

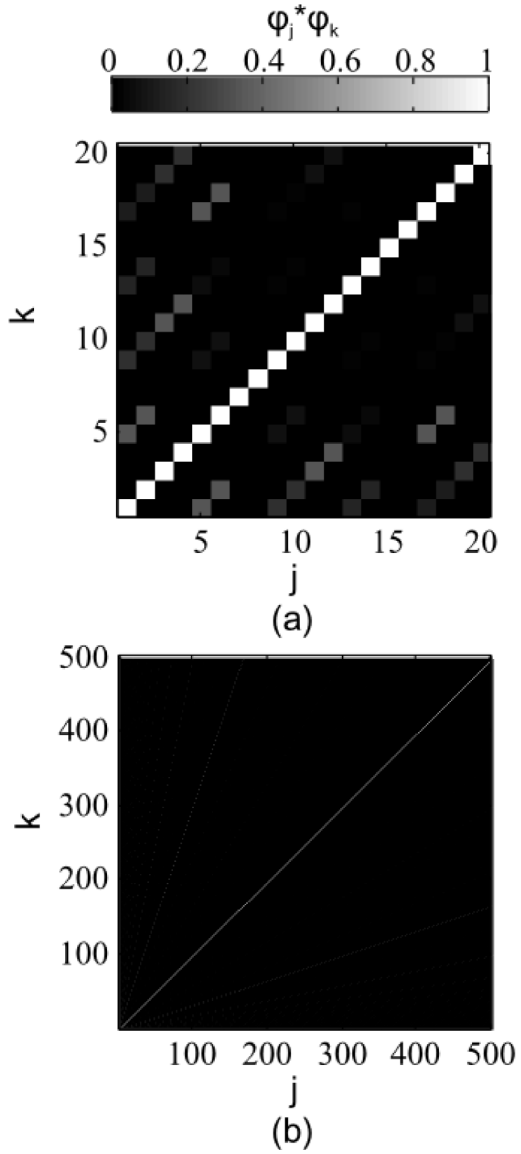

FIG. 8. Elements of the matrix $A_{jk}(=\varphi_j * \varphi_k)$. (a) $1 \le j,k \le 20$ and (b) $1 \le j,k \le 500$.

APPENDIX: MATHEMATICAL COMMENTS ON BASIS FUNCTION sgn{sin(*iωt*)} AND sgn{cos(*iωt*)}

This paper proposes a series expansion of the detector signal, $F(t)$, using basis function of $\mathrm{sgn}\{\sin(i\omega t)\}$ and $\mathrm{sgn}\{\cos(i\omega t)\}$ $(i = 1,2,\ldots)$. This section provides a validity of the basis function. However, since this paper is not a mathematical one, only some evidences of the linear independence will be shown.

Hereafter, let ω be 1, and $\varphi_j(x)$ is defined by

$$\varphi_j(x) = \begin{cases} \sqrt{\dfrac{1}{2\pi}}\mathrm{sgn}\{\cos(ix)\} & (i = 2j-1) \\ \sqrt{\dfrac{1}{2\pi}}\mathrm{sgn}\{\sin(ix)\} & (i = 2j) \end{cases}. \quad \text{(A1)}$$

Besides, a dot-product of functions, f and g, is expressed by

$$f * g = \int_0^{2\pi} f(x)g(x)dx. \quad \text{(A2)}$$

The functions, $\varphi_j(x)$, need to be linearly independent in order to express the detector signal $F(x)$ uniquely. That is to say, scalars c_j $(j = 1,2,\ldots)$ are not all zero such that

$$\sum_{j=1}^{N} c_j\varphi_j = 0. \quad \text{(A3)}$$

Dot-product of this equation and the functions, φ_j, lead to the simultaneous equations below,

$$\sum_{j=1}^{N} c_j\varphi_j * \varphi_k = 0 \quad (k = 1,2,\ldots,N). \quad \text{(A4)}$$

Let A be defined by

$$A_{jk} = \varphi_j * \varphi_k. \quad \text{(A5)}$$

When the rank of A is equal to N, the functions, φ_j (or, equivalently, $\mathrm{sgn}\{\sin(i\omega t)\}$ and $\mathrm{sgn}\{\cos(i\omega t)\}$), are linearly independent. Fig. 8 shows elements of the matrix A for $N = 20$ and $N = 500$. In the both cases, the rank of A is equal to N. Fig. 8 is an evidence of the linear independence of $\mathrm{sgn}\{\sin(i\omega t)\}$ and $\mathrm{sgn}\{\cos(i\omega t)\}$.

It should be noted that $\mathrm{sgn}\{\sin(i\omega t)\}$ and $\mathrm{sgn}\{\cos(i\omega t)\}$ are not orthogonal because the matrix A is not a unit matrix (as shown in Fig. 8).

[1]A. E. Costley, S. Allen, P. Andrew, L. Bertalot, R. Barnsley, X. R. Duan, A. Encheva, C. Ingesson, D. Johnson, H. G. Lee, Y. Kawano, A. Krasilnikov, V. Kumar, Y. Kusama, E. Marmar, S. Pak, C. S. Pitcher, C. V. S. Rao, G. Saibene, D. Thomas, P. R. Thomas, P. Vasu, G. Vayakis, C. Walker, Q. W. Yang, V. Zaveriaev, and J. Zhao, "Measurement requirements and the diagnostic system on iter: Modifications following the design review," in 22nd IAEA Fusion Energy Conference, Geneva, Switzerland, 2008.
[2]R. Imazawa, Y. Kawano, and Y. Kusama, "A new approach of equilibrium reconstruction for iter," Nucl. Fusion **51**, 113022 (2011).
[3]R. Imazawa, Y. Kawano, T. Akiyama, K. Nakayama, and K. Itami, "Polarization measurement techniques suitable for iter poloidal polarimeter," in *Proceedings of the 41st Plasma Physics Conference on Plasma Physics (EPS2014)* (IOP, Berlin, Germany, 2014), p. P5.008.
[4]G. Vayakis, C. Watts, R. Reichle, M. Walsh, R. Barnsley, L. Bertalot, S. Pitcher, V. Udintsev, E. Veshchev, P. Andrew, R. Bouhamou, and J. Snipes, "Evolution of the iter diagnostic set specifications," in 24th IAEA Fusion Energy Conference, San Diego, USA, 2012.
[5]L. Giudicotti, S. L. Prunty, C. Nyhan, E. Bedin, E. Zilli, and L. D. Pasqual, "A polarization modulation technique for far-infrared polarimetry in large plasmas," Plasma Phys. Controlled Fusion **46**, 681 (2004).
[6]R. Imazawa, Y. Kawano, and Y. Kusama, "Highly accurate approximate solutions of the stokes equation for high electron density and long laser wavelength," Plasma Phys. Controlled Fusion **54**, 055005 (2012).
[7]S. Okajima, K. Kawahata, A. Ejiri, K. Tanaka, Y. Hamada, and J. Fujita, in *Proceedings of the 7th International Symposium on Laser Aided Plasma Diagnostics* (Fukuoka, Japan, 1995), p. 148.
[8]S. Okajima, K. Nakayama, H. Tazawa, K. Kawahata, K. Tanaka, T. Tokuzawa, Y. Ito, and K. Mizuno, "Development of short-wavelength far-infrared laser for high density plasma diagnostics," Rev. Sci. Instrum. **72**, 1094 (2001).
[9]H. Ohkuma, M. Shoji, S. Suzuki, K. Tamura, and T. Yorita, in *Proceedings of EPAC 2006* (Edinburgh, Scotland, 2006), pp. 961–963.